


Review

Application of Quantum Dots for Photocatalytic Hydrogen Evolution Reaction

Xia Gui ^{1,2}, Yao Lu ¹, Qin Wang ¹, Mengdie Cai ^{1,*} and Song Sun ¹ 

¹ School of Chemistry and Chemical Engineering, Anhui University, Hefei 230601, China; gxia1982@outlook.com (X.G.); lu18254780976@163.com (Y.L.); wangqin000217@126.com (Q.W.); suns@ustc.edu.cn (S.S.)

² Anhui Water Conservancy Technical College, Hefei 231603, China

* Correspondence: caimengdie@ahu.edu.cn

Abstract: There is increased interest in the conversion of solar energy into green chemical energy because of the depletion of fossil fuels and their unpleasant environmental effect. Photocatalytic hydrogen generation from water involves the direct conversion of solar energy into H₂ fuels, which exhibits significant advantages and immense promise. Nevertheless, photocatalytic efficiency is considerably lower than the standard range of industrial applications. Low light absorption efficiency, the rapid recombination of photogenerated electrons and holes, slow surface redox reaction kinetics and low photostability are well known to be key factors negatively affecting photocatalytic hydrogen production. Therefore, to construct highly efficient and stable photocatalysts is important and necessary for the development of photocatalytic hydrogen generation technology. In this review, quantum dots (QDs)-based photocatalysts have emerged with representative achievements. Due to their excellent light-harvesting ability, low recombination efficiency of photogenerated electrons and holes, and abundant surface active sites, QDs have attracted remarkable interest as photocatalysts and/or cocatalyst for developing highly efficient photocatalysts. In this review, the application of QDs for photocatalytic H₂ production is emphatically introduced. First, the special photophysical properties of QDs are briefly described. Then, recent progress into the research on QDs in photocatalytic H₂ production is introduced, in three types: semiconductor QDs (e.g., CdS, CdMnS, and InP QDs), metal QDs (e.g., Au, Pt and Ag QDs), and MXene QDs and carbon QDs (CDQs). Finally, the challenges and prospects of photocatalytic H₂ evolution with QDs in the future are discussed.

Keywords: quantum dots; quantum effect; photocatalyst; hydrogen evolution; light harvesting; charge transfer; solar fuel



Citation: Gui, X.; Lu, Y.; Wang, Q.; Cai, M.; Sun, S. Application of Quantum Dots for Photocatalytic Hydrogen Evolution Reaction. *Appl. Sci.* **2024**, *14*, 5333. <https://doi.org/10.3390/app14125333>

Academic Editor: Nuno Silva

Received: 7 May 2024

Revised: 6 June 2024

Accepted: 12 June 2024

Published: 20 June 2024



Copyright: © 2024 by the authors. Licensee MDPI, Basel, Switzerland. This article is an open access article distributed under the terms and conditions of the Creative Commons Attribution (CC BY) license (<https://creativecommons.org/licenses/by/4.0/>).

1. Introduction

With the increase in energy demands and environmental pollution, it is imperative to develop new approaches to acquiring environmentally friendly energy. Hydrogen has attracted remarkable interest as one of the most green and renewable energy sources to substitute non-renewable energy, such as fossil fuels. At the same time, solar energy is also a clean, sustainable and renewable natural energy. The conversion of solar energy into hydrogen fuels has been regarded as one of the most eco-friendly strategies to substitute fossil fuels, and it will greatly alleviate the global energy crisis and environmental pollution [1–5]. Therefore, hydrogen production from water splitting has attracted more and more attention from researchers [6–10]. However, the technology is still far from industrial applicability due to its low photocatalytic efficiency. The development of efficient photocatalysts for H₂ evolution is crucial for the realization of a sustainable energy future. Ongoing research in this field focuses on improving the efficiency, stability, and cost-effectiveness of photocatalytic systems to make them commercially viable and scalable.

In general, three major steps are involved in photocatalytic H₂ production: (1) light absorption by the semiconductor to generate electrons and holes; (2) photogenerated

charge separation and migration; and (3) the photogenerated electrons are reacted with water to produce hydrogen (Figure 1) [8,10]. These three processes determine the overall photocatalytic efficiency of water splitting. The key challenge in photocatalysis is to design semiconductor photocatalysts that can efficiently absorb light, allow photogenerated charge carriers' separation and transfer, and drive the chemical reactions needed for H₂ production. An effective method to reduce recombination and facilitate the surface reaction required for H₂ production involves the cocatalyst loading strategy, undertaken to improve the photocatalytic efficiency of H₂ evolution reactions. A cocatalyst attached to a semiconductor photocatalyst is well known to play important roles in high-efficiency photocatalytic water splitting for H₂ production:

- (i) The cocatalyst can improve light absorption;
- (ii) The cocatalyst can reduce the activation energy or overpotential of the H₂ generation reaction, leading to a fast surface reaction;
- (iii) The cocatalyst can boost the photogenerated charge carriers' separation and transfer;
- (iv) The cocatalyst can suppress photocorrosion and increase the durability of the photocatalyst.

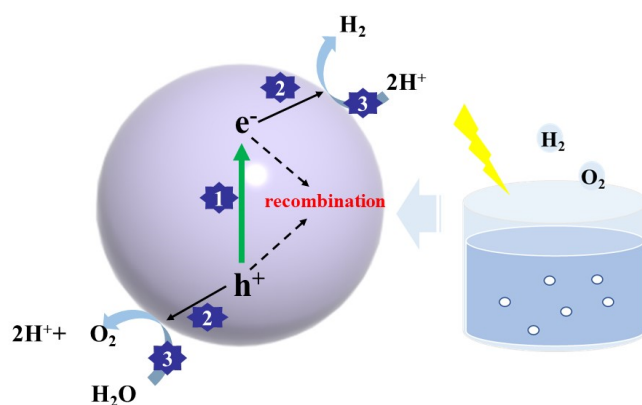


Figure 1. Schematic of water splitting over semiconductor photocatalysts. (1) the light absorption and the formation of the photogenerated electron–hole pairs; (2) the photogenerated carriers migrate to the surface of semiconductor; (3) the photogenerated carriers participate the surface reactions.

Typical H₂ evolution cocatalysts include noble metals such as Pt, Au, and Ag, and transition metals such as Co, Ni, and Cu, as well as transition metal sulfides or phosphides (e.g., MoS₂, WS₂, NiS, Ni₂P, CoP, and FeP and so on), which can trap photogenerated electrons and provide the additional active sites for hydrogen generation. Particularly, noble metals such as Pt nanoparticles, when used as cocatalysts, also have an important promotional effect on the optical properties of the photocatalyst, affecting the surface plasmon resonance (SPR), which could significantly enhance the photocatalytic H₂ generation efficiency.

Notably, the band gap and CB and VB levels are the most important factors determining the performance of a photocatalyst. Generally, the photocatalytic H₂ generation reaction is a thermodynamically feasible process when the CB level of a semiconductor photocatalyst is more negative than the reduction potential of H⁺/H₂ [11]. Therefore, to achieve efficient H₂ evolution efficiency, a semiconductor photocatalyst must fulfill several requirements: (i) high visible light utilization; (ii) low recombination of charge carriers; (iii) the CB level should be greater than the hydrogen reduction potential (H⁺/H₂) level; (iv) it should be stable under extreme environments, and (v) cost-effectiveness. Much effort has been devoted to the search for a photocatalyst that can satisfy these requirements [12–14]. Recent advances have revealed that quantum dots (QDs) demonstrate promise for use in the photocatalytic H₂ evolution reaction because of their unique optical–physical properties, including a good light absorption coefficient, quantum confinement effect, and optical stability.

Due to the quantum-confined effect, QDs have demonstrated promise in efficient photocatalytic reactions. Compared to bulk semiconductor materials, semiconductor QDs show band-gap tunability, good visible light absorption, and more active sites. QDs are

defined as a class of quasi-zero-dimensional (0D) nanoparticles. The exciton Bohr radius is a critical length scale for QDs, as it defines the size range over which QDs exhibit quantum confinement effects. For a given material, QDs must be smaller than this radius so as to exhibit molecular-like behavior [15]. The photophysical properties of QDs, such as absorption, emission wavelength, and quantum yield, can be tuned by controlling their size. As the size of the QDs decreases, the bandgap increases due to quantum confinement, leading to a blue shift in absorption and emission spectra. As the size of the QDs increases, their energy levels begin to merge and form bands similar to those in bulk semiconductors. This leads to properties that are more typical of traditional semiconductor materials, such as a broad emission spectrum and less pronounced quantum confinement effects. As mentioned, Figure 2 illustrates the transition of electronic energy states from discrete molecules to a bulk material, with QDs lying in between these two extremes [16]. In semiconductor QDs, the electron and hole energy states are discrete and regular. Owing to quantization, the band gap of semiconductor QDs is enhanced in comparison with that of bulk semiconductors, with the CB and VB energy levels moving up and down, respectively. Then, the redox potentials of H₂ generation within QDs are easily adjusted by particle size regulation, and quantum confinement endows semiconductor QDs with tunable driving forces to make a majority of the redox reactions thermodynamically feasible. Besides this, compared to bulk semiconductors, QDs exhibit a short electron–hole diffusion distance due to their small size, facilitating the efficient migration of the charge carrier and weakening the adverse effects of interior recombination centers [14,17,18]. Moreover, the abundant surface active sites in QDs speed up the surface reaction, and then enhance the photocatalytic performance. At the same time, the electron transfer (ET) route of semiconductor QDs is flexible, and can be used for the spatially restricted close interactions between electron donor–acceptor sites [19].

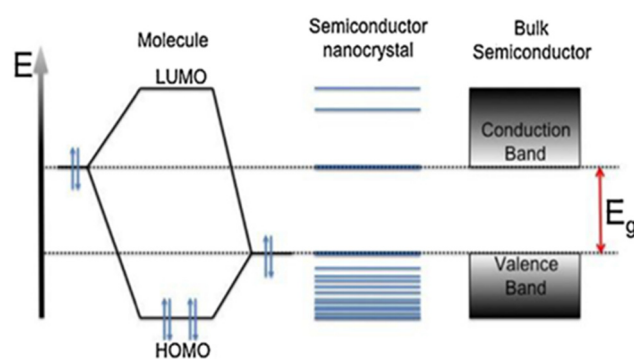


Figure 2. A schematic representation of the electronic energy states of discrete molecules, nanocrystals, and bulk semiconductor materials. Reprinted with permission from Ref. [16].

The quantum confinement effect in QDs has given rise to several fascinating optoelectronic features, leading to good visible light absorption, the rapid migration of charge carriers, and low reduction potentials, which are extremely important for photocatalytic H₂ production [20]. Except for semiconductor QDs, other photoactive metal or metal-oxide QDs and carbon QDs (CQDs) are also potential candidates, as they rely on sunlight for photocatalytic water splitting. In particular, CQDs are promising candidates for use in the development of photocatalysts [21–24], which include delocalized conjugated π structures that can induce the rapid migration of charge carrier, leading to promoted photocatalytic efficiency [25–27]. Meanwhile, CQDs show the special optical property of up-conversion fluorescence emission due to their quantum confinement [27–32], which expands the light-utilization range and improves the photocatalytic efficiency [23,25].

This review summarizes the recent research progress in the application of QDs for photocatalytic H₂ production. The applications of QDs are categorized into three types: semiconductor QDs (e.g., CdS, CuInS₂, and InP), metal QDs (e.g., Ag, Au, and Ni), and

carbon QDs. Finally, challenges and prospects associated with the application of QDs for photocatalytic H₂ production in the future are discussed.

2. Quantum Dots-Based Photocatalyst for Hydrogen Evolution

By summarizing the application of QDs in photocatalytic hydrogen production in recent years, it has been found that the application of QDs in photocatalytic hydrogen evolution can be divided into three categories, which are the use of single semiconductor QDs as photocatalysts; semiconductor–quantum-dot-based hybrid photocatalysts; metal QDs and MXene QDs used as cocatalysts; carbon QDs-based hybrid photocatalysts. Table 1 provides a detailed summary of the reported examples of the QDs utilized for photocatalytic H₂ generation.

Table 1. Cases of recently reported QDs-based photocatalysts used for photocatalytic H₂ generation.

Photocatalyst	Cocatalyst	Reaction Medium	Light Source	H ₂ Generation (mmol h ⁻¹ g ⁻¹)	Referenced Sample/Enhancement Factor ^a	Ref.	QDs Size (nm)
ZnCdS QDs		Na ₂ SO ₃ and Na ₂ S	300 W Xe lamp (λ ≥ 420 nm)	3.70	bulk ZnCdS/5.2	[33]	4.5–7.8
CuInS QDs		ascorbic acid	LED light source (470 nm)	116	Cu ₂ S/18	[34]	3
Cd _{0.67} Mo _{0.33} Se QDs		Na ₂ SO ₃ and Na ₂ S	300 W Xe lamp	0.911	MoSe ₂	[35]	3
CdS QDs		Na ₂ SO ₃ and Na ₂ S	300 W Xe lamp	0.410	Bulk CdS/5	[36]	6
CdSe/CdS/ZnS QDs		Na ₂ SO ₃ and Na ₂ S	300 W Xe lamp	0.195	CdSe QDs/6.32	[37]	7.2
CdSe QDs/g-C ₃ N ₄		L-ascorbic acid	500 W Hg lamp (λ ≥ 420 nm)	0.615	g-C ₃ N ₄ /76	[38]	2–3
CdCO ₃ /CdS QDs		Na ₂ SO ₃ and Na ₂ S	300 W Xe lamp (λ ≥ 420 nm)	1.93		[39]	5
CdS QDs/Pt/In ₂ O ₃	Pt/In ₂ O ₃	Lactic acid	300 W Xe lamp (λ ≥ 420 nm)	1.03		[40]	
CuInS ₂ QDs/CN		Triethanolamine (TEOA)	300 W Xe lamp (λ ≥ 420 nm)	1.92	CN/2.6	[41]	5
ZnAgInS QDs/2D MoS ₂ nanosheet		Ascorbic acid	300 W Xe lamp (λ ≥ 400 nm)	40.1		[42]	3–5
CdSe QDs/WS ₂ nanosheet		Lactic acid	300 W Xe lamp (λ ≥ 420 nm)	14		[43]	7–8
Colloidal CdS/CdSe core/shell QDs		Ascorbic acid	300 W Xe lamp (λ ≥ 420 nm)	AQY ^b : 30.9%	CdS core/1.49	[44]	
NiS QDs/g-C ₃ N ₄	NiS QDs	TEOA	300 W Xe lamp (λ ≥ 420 nm)	0.484	pristine g-C ₃ N ₄ /45	[45]	
MoS ₂ -QDs/ZnIn ₂ S ₄	MoS ₂ -QDs	TEOA	300 W Xe lamp (λ ≥ 420 nm)	7.15	pure ZnIn ₂ S ₄ /9	[46]	8
MoS ₂ -QDs/g-C ₃ N ₄	MoS ₂ -QDs	TEOA	300 W Xe lamp (λ ≥ 420 nm)	1.97	g-C ₃ N ₄ /6.6	[26]	
Co ₃ O ₄ QDs		50 vol% ethanol	300 W Xe lamp (λ ≥ 420 nm)	1.1	Bulk Co ₃ O ₄ (No activity)	[47]	3–4
0D Co ₃ S ₄ QD/2D g-C ₃ N ₄ nanosheets	Co ₃ S ₄ QDs	TEOA	300 W Xe lamp (λ ≥ 400 nm)	20.5	g-C ₃ N ₄ nanosheets/555	[48]	2–4
Co ₃ O ₄ QDs/TiO ₂ nanobelts	Co ₃ S ₄ QDs	10 vol% methanol	300 W Xe lamp (cut by 1.5 AM filter)	1.74	TiO ₂ nanobelts/1.3	[49]	3
NiO QD/TiO ₂	NiO QDs	10 vol% methanol	300 W Xe lamp	1.35	pure TiO ₂ /56	[50]	2
Ni ₂ P QD/red P	Ni ₂ P QDs	10 vol% methanol	300 W Xe lamp (λ ≥ 420 nm)	0.27	Red P/38.5	[51]	7

Table 1. Cont.

Photocatalyst	Cocatalyst	Reaction Medium	Light Source	H ₂ Generation (mmol h ⁻¹ g ⁻¹)	Referenced Sample/Enhancement Factor ^a	Ref.	QDs Size (nm)
Ni ₂ P QDs/g-C ₃ N ₄	Ni ₂ P QDs	TEOA	300 W Xe lamp (λ ≥ 420 nm)	1.51	pure g-C ₃ N ₄ /11	[52]	4–5
g-C ₃ N ₄ @Ti ₃ C ₂ QDs	Ti ₃ C ₂ QDs	TEOA	300 W Xe lamp with a 1.5 AM filter	5.12	g-C ₃ N ₄ /26	[53]	
Au QDs/rimous CdS nanospheres	Au QDs	Na ₂ S and Na ₂ SO ₃	300 W Xe lamp (λ ≥ 420 nm)	0.60	CdS nanospheres/1.8	[54]	3.5
Ag QDs/g-C ₃ N ₄	Ag QDs	20 vol% methanol	300 W Xe lamp (λ ≥ 420 nm)	0.0181	g-C ₃ N ₄ /4.6	[55]	
CDs/g-C ₃ N ₄	CDs	TEOA	300 W Xe lamp (λ ≥ 420 nm)	2.34	g-C ₃ N ₄ /4.6	[56]	4
CQDs/g-C ₃ N ₄	CQD	Methanol	300 W Xe lamp (λ ≥ 420 nm)	3.54	g-C ₃ N ₄ nanotubes/2.5	[28]	
CQDs/TiO ₂	CQDs	Methanol	500 W halogen lamp (λ ≥ 450 nm)	0.0085	TiO ₂ /4	[30]	4–6
P-TCN ^c /GQDs	GQDs	20 vol% methanol	300 W Xe lamp (λ ≥ 420 nm)	1.12	bulk carbon nitride/9	[57]	
Ag/CQDs/g-C ₃ N ₄	Ag/CQDs	TEOA	300 W Xe lamp (λ = 400 nm)	0.627	g-C ₃ N ₄ /6.7	[58]	2.59
Pt QDs/BiOBr	Pt QDs	Na ₂ S and Na ₂ SO ₃	300 W Xe lamp	0.0320	BiOBr/143	[59]	
Ni QDs/CdS	Ni QDs	Lactic acid	300 W Xe lamp (λ > 420 nm)	10.3	CdS/30	[60]	5.1
CdS QDs/UiO-66		Na ₂ S and Na ₂ SO ₃	225 W Xe light (λ > 420 nm)	15.32	UiO-66-(SH) ₂ /CdS/25.3	[61]	1
MoS ₂ QDs/Cs ₃ Bi ₂ I ₉	MoS ₂ QDs	Ethanol, HI/H ₃ PO ₂ mixed solution	300 W Xe lamp (λ > 420 nm)	6.09	Cs ₃ Bi ₂ I ₉ /9.8	[62]	2–5
N-GQDs/PUCN ^d	N-GQDs	TEOA	300 W Xe lamp (λ ≥ 400 nm)	0.529	PUCN/208	[63]	

^a Compared with the reference sample, the enhancement factor of the photocatalytic performance. ^b AQY: apparent quantum yield. ^c P-TCN: phosphorus-doped hexagonal tubular carbon nitride. ^d 0 D nitrogen-doped graphene quantum dots (N-GQDs) on 2D porous ultrathin carbon nitride (PUCN).

A semiconductor particle smaller than its Bohr exciton diameter can exhibit quantum confinement effects, which distinguish QDs from their bulk counterparts. In this case, the charge carriers become spatially confined, such that the energies of photogenerated electrons and holes are increased. As shown in Figure 3a, bulk CdSe has a moderate bandgap ($E_g = 1.74$ eV), while 2.0 nm CdSe particles have a notably large bandgap (2.88 eV). The conduction band energy (E_{CB}) is increased (electrons in the conduction band become more reduced), and the valence band energy (E_{VB}) is decreased. Smaller QDs are thus expected to more easily engage in interfacial electron transfer with H₂ evolution cocatalysts than larger QDs. Indeed, according to Marcus theory, quantum confined systems can exhibit high rates of interfacial charge transfer owing to the increased energies of confined electron–hole pairs, which is of benefit to applications in solar-to-fuel conversions, such as artificial photosynthetic H₂ evolution. While bulk CdSe and 6.0 nm QDs are not excellent photocatalysts, the smaller particles are, with their normalized rate of H₂ evolution increasing when smaller QDs are used (Figure 3b). Therefore, it is clear that optimizing QD size distribution is an effective and facile pathway to increasing the rate of solar H₂ evolution from QD-based photosystems [15].

Semiconductor QDs typically comprise group II–VI, III–V, or IV–VI elements. In a majority of cases, semiconductor QDs serve as light absorbers to capture solar light during photocatalytic reactions. Moreover, owing to the small size of QDs, they exhibit not only a short electron–hole diffusion distance that facilitates the efficient separation of electron–hole

pairs and weakens the adverse effect of interior recombination centers, but they also show also abundant surface sites that accelerate H₂ production.

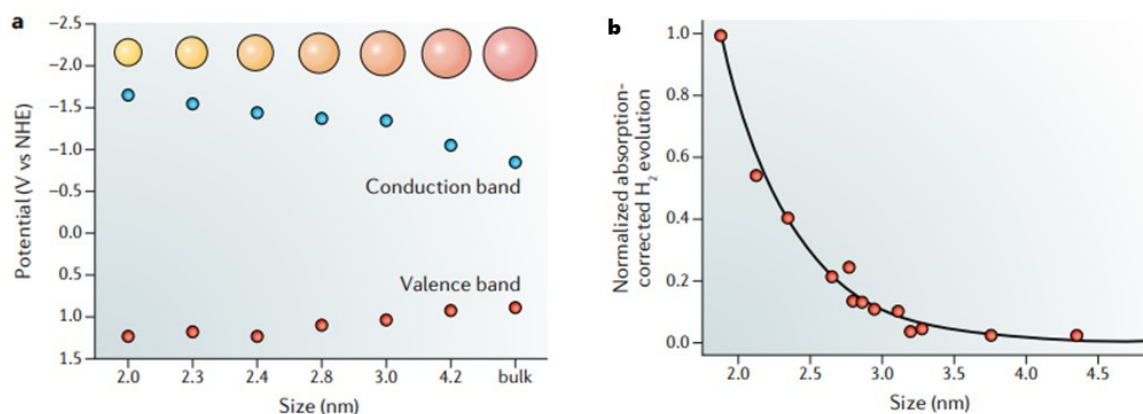


Figure 3. Quantum confinement effect in controlled photocatalytic H₂ evolution. (a) The potentials of the conduction and valence bands of CdSe change as the sizes of the particles vary from nanoscale to bulk. The upper circles illustrate the corresponding size variation. (b) The relative photocatalytic H₂ evolution rates are normalized with regard to photocatalyst sizes. Reprinted with permission from Ref. [15].

2.1. Single-Semiconductor QDs as Photocatalyst

Just like the traditional semiconductor photocatalyst, semiconductor QDs alone can directly act as a photocatalyst in the H₂ evolution reaction; at the same time, they can also combine with other semiconductors or photocatalysts for use as materials to prepare hybrid photocatalysts for H₂ evolution reactions, which we will discuss in the next part. Transition metal sulfide quantum dot nanocrystals with large absorption coefficients, abundant active sites and quantum-limited domain effects are emerging as solar energy utilizers [64]. As well-known IIB-VI semiconductors, CdS photocatalyst systems have been extensively investigated for use in photocatalytic H₂ generation from water because of their special advantages, including their controllable morphology and suitable band gap. Hydrothermal and solvothermal methods are commonly used for the preparation of CdS [65–68]. However, one of the more challenging aspects is the fast recombination of photogenerated charge carriers on the bulk CdS photocatalyst, which can easily lead to low photocatalytic activity [69,70]. In this regard, CdS QDs with small particle sizes shows unique advantages, including the rapid migration of photogenerated electrons to the surfaces of CdS, the abundance of surface active sites, and the quantum confinement effect, which could effectively promote the separation efficiency of photogenerated charge carriers and further enhance the photocatalytic performance; therefore, the application of semiconductor QDs is extensive in photocatalytic H₂ production [71,72].

For example, Jiang et al. [36] reported that mono-metal sulfide (MS) (M = Cd, Zn) QDs prepared via a modified gel crystal growth method exhibit higher H₂ evolution rates than those of bulk MS, corresponding to the synergistic effects of the QDs and the hydrogel. MS QDs demonstrate unique light absorption due to their extremely small size, compared with bulk MS photocatalysts. The unique up-conversion fluorescence effects of MS QDs extend the light absorption range and maximize the light absorption efficiency. Similarly, Fan et al. [73] employed a simple effective method to enhance the photocatalytic H₂ evolution of CdSe QDs; after the surface modification with partial coverage of ZnS, the CdSe QDs exhibited high photocatalytic activity with a H₂ generation rate of 306.3 $\mu\text{mol mg}^{-1} \cdot \text{h}^{-1}$. Li et al. [74] reported that the fluorescence efficiency of molybdenum disulfide quantum dots (MoS₂ QDs) could be improved by monoatomic metal (Au, Ag, Pt, Cu) modification, and the fluorescence emission of MoS₂ QDs was enhanced by a factor of 4 under monoatomic Au modification.

Compared to mono-metal chalcogenide QDs, multi-metal chalcogenide QDs can efficiently adjust the band gap through composition control, improving visible light utilization. Thus far, various ternary QDs, such as CdMoSe, CdTeSe, and CdZnSe, have been thoroughly investigated [35,75–77]. The light absorption and band gap of $\text{Cd}_{1-x}\text{Zn}_x\text{S}$ as a representative can be tuned by the alteration of cationic mole ratios [78]. Similarly, Han et al. [35] prepared aqueous ternary $\text{Cd}_x\text{Mo}_{1-x}\text{Se}$ QDs via the modulation of the metal content, and revealed that the doping of Mo promotes the migration of photogenerated electrons of CdSe QDs, and leads to high photocatalytic activity. Moreover, the $\text{Cd}_{0.67}\text{Mo}_{0.33}\text{Se}$ QDs exhibited good stability in recycling tests.

Li et al. [34] reported that the CuInS_2 QDs with Ru can be used as cocatalysts for photocatalytic H_2 generation, and their photocatalytic performance has been greatly improved, with an apparent quantum yield of 4.7% with Ru deposited on the surface of CuInS_2 QDs. Chen et al. [79] reported a facile method for the controllable preparation of ZnCdS QDs. The as-obtained $\text{Zn}_{0.5}\text{Cd}_{0.5}\text{S}$ QDs with suitable particle sizes, appropriate band matching, and abundant active sites facilitated the separation and transportation of charge carriers and exhibited significantly strong photocatalytic performance.

Perovskite semiconductor QDs have attracted much attention due to their excellent light response and photoluminescence properties that are valuable for photocatalytic H_2 production. For instance, Fan et al. [80] prepared $\text{Cu}_x\text{In}_y\text{S}$ QDs via a hot-injection method, and the $\text{Cu}_x\text{In}_y\text{S}$ QDs with optimized stoichiometric ratios of Cu and In achieved a maximum H_2 production rate of $256 \text{ mmol g}^{-1}\cdot\text{h}^{-1}$. Another kind of perovskite semiconductor QDs is represented by CsPbBr_3 QDs. Notably, the photocatalytic H_2 production was significantly affected by the surface ligands of CsPbBr_3 QDs. For example, Xiao et al. [81] regulated the surface ligand density to optimize the photocatalytic performance. Under visible light irradiation, CsPbBr_3 QDs/ Pt-TiO_2 with different thicknesses of the protective layer showed totally differently photocatalytic activities and selectivities. Meanwhile, Song et al. [33] reported that the monodispersed CsPbBr_3 QDs@PANI prepared by the photopolymerization method showed excellent properties in relation to photocatalytic water splitting performance, with the aid of the conductive polymer PANI as the encapsulating material.

2.2. Semiconductor–Quantum-Dot-Based Hybrid Photocatalyst

Similar to a majority of conventional semiconductor photocatalysts, the photocatalytic performance of single-semiconductor QDs alone is typically limited. One of the most important reasons for this is that the short electron–hole diffusion distance in small-sized QDs easily leads to the recombination of the photogenerated charge carriers before their migration to the surface active sites. Other causes may include a low light-harvesting capability, and the slow kinetics on the QDs' surface. To address these issues, researchers have realized that utilizing semiconductor QDs alone is insufficient for achieving efficient photocatalytic H_2 evolution. Therefore, a hybrid photocatalyst consisting of semiconductor QDs and other chemical materials has been developed and prepared, which exhibits some unique characteristics, such as good solar light utilization and the rapid migration of photogenerated charge carriers; thereby, an improved photocatalytic H_2 generation efficiency can be obtained from the hybrid photocatalyst.

2.2.1. Metal-Chalcogenide-QD-Based Hybrid Photocatalyst

Various IIB–VI semiconductor QDs are frequently used to form composites with other semiconductor photocatalysts to enhance the photocatalytic activity in the visible spectrum due to their special optical–electrical and size-tunability properties, corresponding to quantum confinement effects, which can solve issues of low solar energy utilization and high carrier recombination, in turn achieving the band structure engineering of semiconductors and improving the photocatalytic efficiency [72,82–85]. For example, CdS QDs have been combined with g- C_3N_4 to improve photocatalytic hydrogen evolution efficiency. Cao et al. [85] reported a strategy of growing CdS QDs in situ on a g- C_3N_4 nanosheet surface, leading to the formation of a contact interface between g- C_3N_4 and CdS QDs,

in turn leading to the effective charge carriers' separation on both parts. On the other hand, the hybrid photocatalyst showed an increased number of photocatalytic reactive sites. Consequently, the resultant CdS QD/g-C₃N₄ demonstrated significantly enhanced photocatalytic performances compared with pure g-C₃N₄. Jiao et al. [86] synthesized a novel MoS₂ quantum dot-modified g-C₃N₄ nanosheets/n-doped carbon dot heterojunction photocatalyst via the thermal polymerization and subsequent solvothermal method. The photocatalytic hydrogen precipitation rate of the composite was 212.41 μmol g⁻¹ h⁻¹, which is 53 times higher than that of g-C₃N₄/MoS₂-3%.

Similarly, Ge et al. [13] reported that g-C₃N₄ decorated with CdS QDs exhibits effective photocatalytic performance with a H₂ evolution rate of 17.27 μmol·h⁻¹ under visible light irradiation. This value is 9 times that of pure g-C₃N₄, corresponding to the efficient separation and transportation of the photogenerated charge carriers. Moreover, the CdS QD/g-C₃N₄ composite exhibits red-shift and strong absorption in the visible light region due to the introduction of CdS QDs.

Zhu et al. [87] deposited CdS QDs on TiO₂ nanotube arrays (TNTAs) for visible-light-driven hydrogen production. The optimal CdS-TNTA sample exhibited the highest activity for H₂ generation, which can be explained by the fact that the introduction of CdS QDs could effectively enhance the visible light absorption and charge separation. However, excess CdS QDs easily lead to the formation of CdS particles. Similarly, with CdSe QDs, Chen et al. [88] synthesized and carefully characterized {001}-TiO₂/CdSe QD and {101}-TiO₂/CdSe QD composites using mercaptopropionic acid as the linker. The photocatalytic activity of {001}-TiO₂/CdSe QDs is greater than that of {101}-TiO₂/CdSe QDs in relation to photocatalytic H₂ generation because of the fast migration of photogenerated electrons from the QDs to the {001}-TiO₂.

Pan et al. [40] reported a series of CdS QD/Pt/oxides for use in photocatalytic H₂ evolution, which exhibited superior photocatalytic performance to Pt/CdS, Pt/Ga₂O₃, and Pt/In₂O₃. Among these, CdS/Pt/In₂O₃-U demonstrated the highest photocatalytic activity and excellent stability due to the fast separation and transfer of the photogenerated charge carriers with the aid of CdS QDs.

In addition, ternary metal sulfide is a conventional photocatalytic hydrogen production catalyst; therefore, several researchers have investigated the combination of CdS QDs with ternary metal sulfide to improve the hydrogen evolution activity. For example, Hou et al. [72] reported that CdS QD/graphene/ZnIn₂S₄ composites exhibit excellent photocatalytic performance, with a H₂ production rate of 2.7 mmol·h⁻¹, due to the improved light absorption ability and the facilitated migration of photogenerated electrons resulting from the combination of CdS QDs and ZnIn₂S₄. At the same time, the as-synthesized CdS QD/graphene/ZnIn₂S₄ composite displays good stability, resulting from the high hydrothermal stability and the strong interaction between CdS QDs and ZnIn₂S₄.

Yu et al. [89] prepared a CdS QD-sensitized Zn_{1-x}Cd_xS composite via a simple ion exchange route, and reported the especially high visible light photocatalytic H₂ production rate of 2128 μmol g⁻¹·h⁻¹; this value is 53 times higher than that for CdS. It is also considerably greater than that for Pt/ZnS under both ultraviolet and visible light irradiation. The blue-shift in the absorption spectrum confirms the quantum size effect exhibited by CdS QDs; the introduction of CdS QDs modifies the energy levels of the conduction band (CB) and the valence band (VB) within the combined semiconductor structure, which facilitates electron transfer (ET) and amplifies the photocatalytic efficiency.

Larsen et al. [90] proposed a CdSe/CdS QDs core/shell heterostructure via the growth of a layer of CdS on the surface of the CdSe QDs, and reported significantly improved hydrogen evolution efficiency. Transient absorption spectroscopy revealed the presence of several deep trap states on the pristine CdSe QD surface (Figure 4). These defect states could not produce H₂ because of the lower CB level than is necessary for H₂O reduction. Through the growth of a CdS shell on the surface of the CdSe QDs, the deep trap states can be effectively passivated. Therefore, an increased number of electrons can be maintained at the CB and react with H⁺ to produce hydrogen.

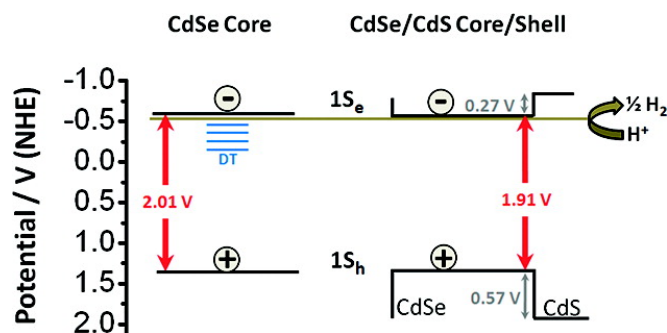


Figure 4. Schematic and photocatalytic activity of CdSe/CdS heterostructure QDs. Reprinted with permission from Ref. [33].

Thus far, Cd-based IIB–VI QDs have been frequently applied in photocatalytic H₂ generation. However, the toxicity of Cd may limit their further application. Therefore, researchers have gradually developed Cd-free QDs to replace Cd-based QDs, and some of these QDs have provided impressive results that are comparable to those of Cd-based QDs. For instance, Xue et al. [71] reported a NiS₂ QDs/g-C₃N₄ composite with the NiS₂ QDs anchored on g-C₃N₄ nanosheets, exhibiting a significantly high photocatalytic efficiency with the hydrogen generation rate of 4.841 μmol·h⁻¹, which value is nearly two times greater than that of the Pt/g-C₃N₄ photocatalyst. Moreover, the composite exhibits high stability. From the results, we can see that NiS₂ QDs act as a cocatalyst to improve the photogenerated charge carriers' separation efficiency, and to increase the surface's active sites, leading to accelerated H₂ generation.

Complex I–III–VI QDs, such as CuInS₂ and ZnS-AgInS₂ QDs, have been widely studied for use in photocatalytic H₂ evolution. The traditional method of preparation for ternary and multinary I–III–VI QDs is the hot injection method. An example of the hot injection method of Zn_xCu_y-InS_{1.5+x+0.5y} QDs is the reaction of metal acetate and sulfur in octadecene with oleic acid and dodecanethiol used as capping reagents. Aqueous synthesis methods are receiving more and more attention because of the promising biological and catalytic applications of I–III–VI QDs. With mercaptoacetic acid, mercaptopropionic acid and other thiol-containing amines/alcohols as ligands, different types of I–III–VI QDs can be synthesized. Zheng et al. [41] synthesized CuInS₂/CN heterojunctions for photocatalytic water splitting. The photocatalytic H₂ evolution activity of the CuInS₂/CN composite is two times greater than that of pure CN, and the improved performance is due to the increased efficiency in separating photogenerated electron–hole pairs and the enhanced capacity to absorb visible light in the CuInS₂/CN hybrid photocatalyst. Liu et al. [42] reported Zn-Ag-In-S QDs combined with a 2D MoS₂ nanosheet for hydrogen generation. The photoluminescence studies show the rapid migration of photogenerated charge carriers between Zn-Ag-In-S QDs and MoS₂ nanosheet, which result in a remarkably high photocatalytic efficiency, with the H₂ production rate of 40.1 mmol g⁻¹·h⁻¹.

2.2.2. Metal-Oxide-QD-Based Hybrid Photocatalyst

Except for metal chalcogenide QDs, a variety of metal oxide QDs including CuO, NiO, Co₃O₄, SnO₂, WO₃, and Bi₂O₃ have been explored for use as cocatalysts in the photocatalytic H₂ production reaction [49,50,91,92]. In general, metal oxide quantum dots have higher photostability than sulfide/selenide quantum dots. Metal oxide quantum dots with low toxicity and good chemical stability have emerged as potential host catalysts for photocatalytic HER [93]. Liu et al. [46] reported that a heterostructure created by the in situ seed-directed growth of MoS₂ quantum dots within ZnIn₂S₄ not only establishes heterojunctions between MoS₂ and ZnIn₂S₄ to spatially separate photogenerated electron–hole pairs, but also provides active sites for electron trapping to promote hydrogen evolution. Consequently, the MoS₂-QD/ZnIn₂S₄ composite achieves a high photocatalytic H₂ evolution rate of 7152 μmol h⁻¹·g⁻¹, which is ~9 times greater than that of pristine

ZnIn₂S₄. MoS₂-QDs serve as a hydrogen evolution reaction cocatalyst and an electron transfer bridge. Similarly, Yang et al. [48] have designed and synthesized high-dispersion transition metal sulfide (Co₃S₄) QDs instead of noble metal cocatalysts to anchor onto g-C₃N₄ nanosheets. As-synthesized Co₃S₄/g-C₃N₄ nanosheet (CNNS) nanohybrids exhibit abundant surface active sites and the fast migration of photogenerated electrons because of the highly dispersed cocatalyst Co₃S₄ QDs; therefore, the Co₃S₄/CNNSs exhibit a remarkably high photocatalytic efficiency, with a photocatalytic H₂ generation rate of 20.5 mmol/g/h, which value is 555 times higher than that of pure CNNS.

Hong et al. [50] developed a facile sacrificial coating method to fabricate a NiO QD/TiO₂ heterojunction. The as-prepared NiO QD/TiO₂ exhibited an excellent H₂ evolution rate of 1.35 mmol h⁻¹·g⁻¹, which is 37 times greater than that of NiO/TiO₂, 56 times greater than that of pure TiO₂, and even approaches that of Pt/TiO₂. This excellent photocatalytic performance results from the small sizes of NiO QDs, which lead to a shorter transfer distance for photogenerated carriers and more surface active sites in the NiO QD/TiO₂ composite than that of NiO/TiO₂. Liu et al. [49] reported that the Co₃O₄ QD/TiO₂ heterojunction exhibits a good photocatalytic performance. The Co₃O₄ QDs act as cocatalyst, play dual roles in photocatalysis to improve the visible light utilization, and tune the work function of TiO₂ to accelerate the H₂ production rate on the Co₃O₄ QDs' surface. In addition, the holes in TiO₂ lead to the generation of oxygen. The mechanism of the overall water splitting by the Co₃O₄ QDs/TiO₂ composite is displayed in Figure 5.

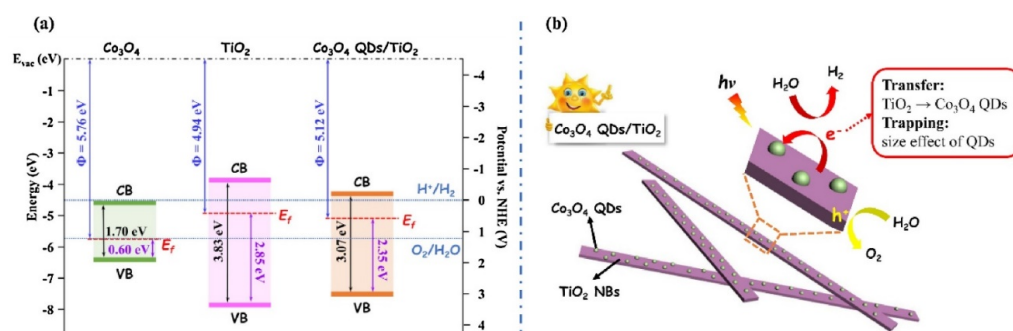


Figure 5. (a) Schematic diagram of the energy band structure; (b) The mechanism by which Co₃O₄ QDs/TiO₂ achieves photocatalytic overall water splitting. Reprinted with permission from Ref. [49].

Pan et al. [92] fabricated tunable Z-scheme semiconductors comprising TiO₂-supported WO_{3-x} QDs by in situ solvothermal and hydrogen reduction methods. The synthesized hybrid photocatalyst exhibited improved photocatalytic performance. This improvement could be related to the formation of W⁵⁺/VO defects at the interface, which are crucial for the fabrication of Z-scheme photocatalysts. Lakshmana et al. [94] reported that Bi₂O₃ clusters@TiO₂ (BT) nanostructures facilitate the enhancement of the photocatalytic H₂ evolution rate. Here, as a cocatalyst, Bi₂O₃ favorably utilizes the excited CB electrons of TNS. The photocatalytic activity of BT and the reproducibility of its performance for five recycles are attributed to the efficient separation of photogenerated charge carriers.

2.2.3. Metal-Phosphide-Quantum-Dot-Based Hybrid Photocatalyst

Metal phosphides (MxPy) have attracted much attention in the context of photocatalytic H₂ evolution from water splitting because of their low hydrogen evolution overpotential, tunable electronic structure, high electrical conductivity, and low price. They can not only act as photocatalysts—GaP and InP are well-known semiconductors—but they can also act as cocatalysts, with NiP and Fe₂P exhibiting metallic behavior. Metal phosphide QDs are new cocatalysts that are attractive for their use in photocatalytic H₂ generation. For example, Liang et al. [51] reported on a Ni₂P QD/red P nanosheet photocatalyst with a p–n heterojunction that exhibited an excellent photocatalytic hydrogen generation rate. The results show that the internal electric field of the p–n heterojunction and the small size of uniform Ni₂P QDs lead to the improved photocatalytic activity of

the Ni₂P QD/red P nanosheets composite. During photocatalysis, the electrons in the CB of Ni₂P QDs are rapidly transferred to red P nanosheets, after which H⁺ is reduced to H₂. The photogenerated holes in the VB of red P are transferred to the Ni₂P QDs, and then oxidize the sacrificial agents (Figure 6). In addition, Ni₂P QDs are synthesized and highly dispersed on the red P nanosheet's surface, affording abundant photocatalytically active sites. Jia et al. [95] achieved efficient photocatalytic H₂ precipitation via the in situ loading of Ni single-atom sites onto RP QDs; the presence of nickel atoms significantly lowered the energy barrier for electron transfer in the photocatalytic process. The Ni-P sites acted as electron antennae to attract light carriers to the solid–liquid interface, which activated the protons to initiate the effective H₂ production process, resulting in a high rate of H₂ production—224-fold higher than that of the original RP QDs.

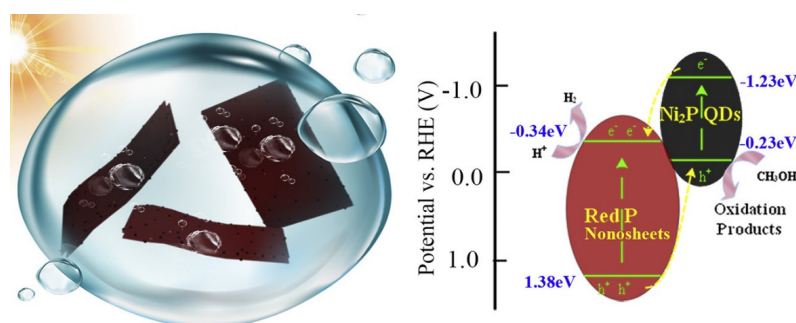


Figure 6. The photocatalytic mechanism of the Ni₂P QD/red P nanosheets hybrid used for photocatalytic hydrogen production. Reprinted with permission from Ref. [51].

Researchers have extensively explored InP-based photocatalysts for use in photocatalysis due to their adjustable band gaps, high absorption coefficients, narrow emission line widths, and flexible composition [94,96]. Furthermore, InP exhibits a more significant degree of covalent bonding than cadmium selenide (CdSe), resulting in decreased electron–hole attraction and reduced photon coupling. Recently, InP quantum dots (QDs) have been utilized for photocatalytic hydrogen (H₂) production. Greta and Wu et al. [97] have investigated InP/ZnS QDs for use in photocatalytic H₂ generation. By covering the surface of the InP QD with ZnS, the hydrogen evolution rate was enhanced compared with blank InP QDs. Under optimal conditions, an internal quantum yield of 31% at 525 nm can be achieved.

2.2.4. MXenes-QDs-Based Hybrid Photocatalyst

As new 2D materials, MXenes have attracted remarkable interest due to their excellent electrical conductivity, hydrophilic property, and abundant surface functional groups [98–100]. Therefore, MXene can be used as a novel cocatalyst. As a well-known MXene, Ti₃C₂ has been widely explored for photocatalytic H₂ generation [53]. In particular, 0D Ti₃C₂ QDs have attracted more notable attention due to their abundant active edge sites compared with the 2D Ti₃C₂ sheets [53,100]. Zhou et al. [101] categorized MXene QD synthesis methods as top-down and bottom-up, with precursors in top-down methods typically split by physical, chemical or electrochemical methods, while bottom-up methods use small-molecule organic and inorganic precursors, which are then converted into appropriately sized QDs. Thus far, Ti₃C₂ has generally been prepared in 2D NSs and combined with other semiconductors to enable efficient photocatalytic H₂ production. Few studies have focused on the design and photocatalytic applications of Ti₃C₂ QDs. Li et al. [53] mixed and freeze-dried g-C₃N₄ with Ti₃C₂ MXene QDs in order to use them as an efficient catalyst for photocatalytic H₂ generation. The results show that g-C₃N₄@Ti₃C₂ QDs hybrid photocatalysts exhibit a remarkably enhanced solar light conversion efficiency, with a H₂ generation rate of 5111.8 μmol g⁻¹·h⁻¹, which is nearly 26, 3, and 10 times greater than those of g-C₃N₄ NSs, Pt/g-C₃N₄, and the Ti₃C₂ MXene sheet/g-C₃N₄, respectively. Using a Ti₃C₂ QD with tiny particle size as the cocatalyst led to an increased number of

surface active sites, and improved the migration of photoexcited electrons due to the close contact between Ti_3C_2 QDs and $\text{g-C}_3\text{N}_4$ NSs; thus, the electrons could participate in rapid photocatalytic H_2 evolution (Figure 7).

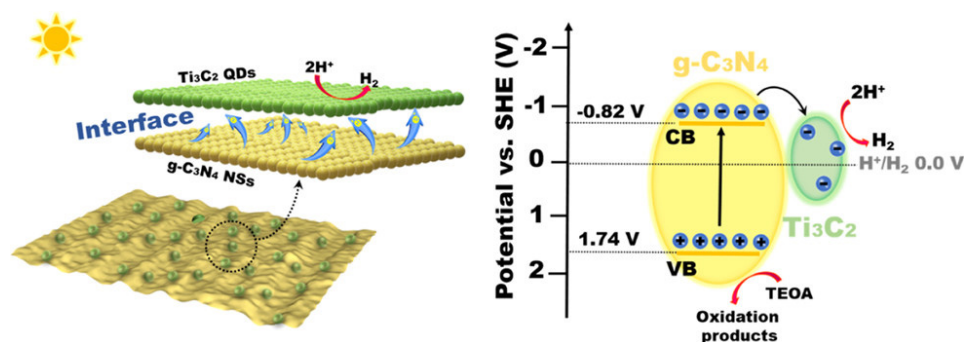


Figure 7. The photocatalytic mechanism of $\text{g-C}_3\text{N}_4@ \text{Ti}_3\text{C}_2$ QD composites. Reprinted with permission from Ref. [53].

2.3. Metal-QD-Based Hybrid Photocatalyst

Recently, hybrid photocatalysts with noble metal QDs as cocatalysts are being widely investigated by researchers [102]. Noble metal QDs such as Au, Ag, and Pt QDs can serve as antennae to capture photogenerated electrons from the CB of semiconductor photocatalysts, accelerate the migration of charge carriers, and consequently improve photocatalytic efficiency [103–105]. Moreover, due to the unique localized SPR effect, noble-metal QDs can efficiently improve the solar light absorption ability, then contribute to the improvement of photocatalytic performance [54,55,102–107]. For instance, Kuang et al. [54] have reported on the use of a simple hydrothermal process, followed by photoreduction, to synthesize hybridized photocatalysts with gold quantum dots embedded in cadmium sulfide nanospheres. The fabricated Au–CNS hybrids show an improved photocatalytic hydrogen evolution rate. In addition, their stability is also enhanced because of the chemical stability and the rapid migration of photogenerated electrons from CNSs to Au QDs. Here, a rough surface and irregular fissures are crucial to anchoring Au QDs onto the CNSs, and then the strong interaction between Au QDs and CNSs lead to the rapid separation of charge carriers and further improve the photocatalytic efficiency. Zhang et al. [55] have reported that Ag QDs/ $\text{g-C}_3\text{N}_4$ (Ag QDs/ $\text{g-C}_3\text{N}_4$) photocatalysts exhibit a higher photocatalytic H_2 evolution rate than blank $\text{g-C}_3\text{N}_4$ due to the extension of the solar light absorption by coupled Ag QDs, which can act as a $\text{g-C}_3\text{N}_4$ electron reservoir for the effective separation of photoexcited electron–hole pairs, further increasing the photocatalytic efficiency of Ag QDs/ $\text{g-C}_3\text{N}_4$.

2.4. Carbon Quantum Dots Based Hybrid Photocatalyst

Carbon quantum dots (CQDs) are 0D carbon nanomaterials with a conjugated π structure; they comprise sp^2/sp^3 hybridized carbon atoms, and exhibit unique optical properties and electrical properties [107]. These CQDs exhibit special characteristics, including broad optical absorption and the up-conversion of fluorescence emissions [27,29,108]. In this regard, CQDs can be used as the cocatalyst for the photosystem, and the development of CQDs-based photocatalysts for H_2 production has attracted immense attention in recent years.

The most fundamental issues in photocatalysis include the low light absorption, fast recombination of photogenerated charge carriers, and slow surface reaction rate within the photocatalysts [8,59]. Here, during photocatalytic H_2 generation with CQDs-based photocatalysts, CQDs can act as a photosensitizer to improve the solar light absorption of the photocatalysts and/or an electron reservoir to inhibit the recombination of charge carriers, resulting in enhanced photocatalytic performance. Hence, various semiconductor photocatalysts have been combined with CQDs to enhance the visible light absorption and improve the migration of photogenerated electron–hole pairs, thus enhancing

photocatalytic efficiency [22,24,25,27]. Moreover, CQDs can even act as single photocatalysts for photocatalysis [28].

For example, CQDs serve as a cocatalyst in the photocatalytic H₂ generation reaction. They can reserve electrons from the photocatalyst to improve efficiency via the rapid migration of photogenerated electron–hole pairs. Typically, CQDs serve as a reservoir for electrons to improve efficiency via the separation of electron–hole pairs in TiO₂. Yu et al. [108] prepared GQDs via the alkali-mediated hydrothermal method, and CQDs/(001)-faceted anatase TiO₂ composites were prepared by the further hydrothermal deposition of GQDs on (001) TiO₂ nanosheets for effective photocatalytic H₂ evolution. The results show that CQDs implanted into (001)TiO₂ sheets act as electron traps to accelerate the migration of photogenerated electron–hole pairs, further leading to the improvement of photocatalytic performance. The CQDs/(001)TiO₂ hybrid photocatalyst with 5 wt. % of CQDs exhibits a significantly higher photocatalytic performance, with the H₂ generation rate of 79.3 μmol g⁻¹·h⁻¹, which value is 8 times that of bare (001)TiO₂. Moreover, the CQDs/(001)TiO₂ hybrids exhibit good stability over 30 h. Similarly, Sui et al. [22] reported that CQDs/TiO₂ nanosheets with (001) facets of TiO₂-001 exhibit an excellent photocatalytic performance with a significantly higher H₂ generation rate and long durability. They CQDs were synthesized by the electrochemical method and further combined with TiO₂ nanosheets under heating conditions to produce CQDs/TiO₂-001 photocatalysts. The enhancement in photocatalytic efficiency is attributed to a synergistic effect between the highly active (001) facet of TiO₂-001 and CQDs; the more active facet (001) can promote electron transfer, and the CQDs serve as an electron trap to suppress the recombination of photogenerated charge carriers. Additionally, the integration of CQDs enhances the absorption of visible light, as they function as photosensitizers. The formation of a Ti–O–C bond between CQDs and TiO₂-001 further leads to a yet higher photocatalytic efficiency for CQDs/TiO₂-001. Figure 8 shows the mechanism of photocatalytic H₂ production by CQDs/TiO₂-001 hybrids. Lv et al. [109] employed the open hollow structure and doping strategy to prepare CQDs-doped Fe/Co/Ni phosphides with a unique open hollow structure, which enhanced the spillover rate of the gas phase, increased the number of active centers, and achieved a significant enhancement in seawater electrolysis performance. Wang et al. [28] reported on CQDs/g-C₃N₄ nanocomposites prepared by the in situ synthesis of CQDs on the surface of g-C₃N₄ using urea and glucose precursors, which were investigated for use in photocatalytic H₂ generation. The results show that the as-prepared CQDs/g-C₃N₄ hybrids exhibited an excellent H₂ evolution rate of 2.34 μmol g⁻¹·h⁻¹, which was 4 times greater than that of pristine g-C₃N₄. The enhancement in photocatalytic activity is primarily due to the creation of a built-in electric field at the interface between the carbon quantum dots (CQDs) and graphitic carbon nitride (g-C₃N₄). This built-in electric field significantly improves the separation of photoinduced electron–hole pairs. Furthermore, the close integration of CQDs with g-C₃N₄ forms an effective electron transfer (ET) channel, which enhances the photocatalytic efficiency for hydrogen (H₂) production.

The up-conversion photoluminescence (UCPL) property of CQDs plays a significant role in photocatalysis by enabling the conversion of low-energy photons to higher energy states. This process expands the spectrum of light that is usable for photocatalytic reactions, as it allows near-infrared (NIR) or even infrared (IR) light, which carry lower energy than visible light, to be upconverted to a higher energy level that can be utilized by the photocatalyst. When CQDs were combined with a semiconductor (such as g-C₃N₄), the CQDs not only extended the light response range of g-C₃N₄, but also accelerated the transfer of photoinduced charges by promoting electron excitation to higher energy levels, where they can participate in redox reactions more effectively [58]. Moreover, CQDs could be used as an electron reservoir to effectively improve the photogenerated charge carriers' separation efficiency, even in the NIR region. Wang et al. [28] have reported that the integration of CQDs into g-C₃N₄ affords CQDs-implanted g-C₃N₄ nanotubes (CCTs). Compared with those of g-C₃N₄ and CQDs/g-C₃N₄, the PL emission intensity of CCTs is dramatically decreased, indicating that the CQDs implanted with sp²-hybridized nitrogen

as an electron buffer can considerably facilitate excited electron transfer; this, in turn, further inhibits the recombination of photogenerated electron–hole pairs. Thus, the as-prepared CCTs exhibited increased visible light absorption and decreased the energy barrier of the H_2 generation reaction, showing significantly high photocatalytic performance with a H_2 generation rate of $3538.3 \mu\text{mol g}^{-1}\cdot\text{h}^{-1}$. Chen et al. [110] constructed a system of indium phosphide quantum dots and carbon quantum dots (InP QDs/CQDs), and the average rate of photocatalytic decomposition of hydrogen sulfide for hydrogen production in the InP QDs/CQDs system was increased by a factor of 2.1 compared with that of InP QDs alone, suggesting that the introduction of the CQDs could effectively improve the separation efficiency of the photogenerated carriers.

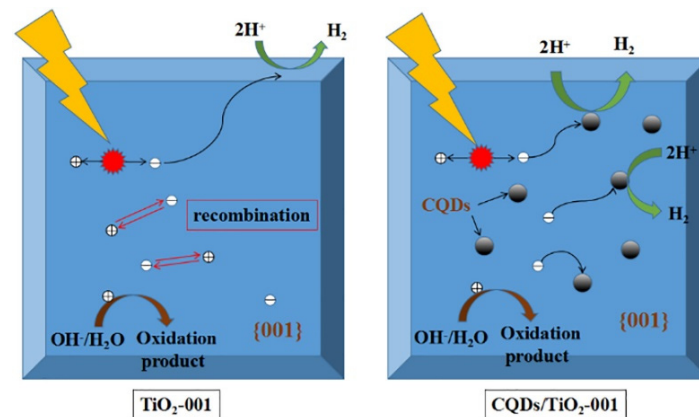


Figure 8. The photocatalytic mechanism of TiO_2 -001 and $CQDs/TiO_2$ -001. Reprinted with permission from Ref. [22].

GQDs are special CQDs that comprise one or a few layers of graphene of a small size ($<10 \text{ nm}$), and exhibit various unique characteristics, including an abundance of surface functional groups and fluorescence properties, and they can serve as cocatalysts to facilitate the migration of photogenerated charge carriers, leading to the improvement of photocatalytic performance [57,111]. Moreover, GQDs can extend the light absorption range as a result of their up-conversion luminescence property. These advantages demonstrate that the modification of GQDs demonstrates promise in relation to the improvement of photocatalytic efficiency in conventional photocatalysts. Lei et al. [111] synthesized $CdS/GQDs$ nanohybrids with “dot-on-particle” heterodimer structures, and the as-synthesized hybrids exhibited a higher H_2 evolution rate of $95.4 \mu\text{mol}\cdot\text{h}^{-1}$, which value is about 4 times greater than that obtained by the CdS photocatalyst. As for the photocatalytic mechanism underpinning the improved photocatalytic performance, the results reveal that GQDs act as cocatalysts for $CdS/GQDs$ nanohybrids, mainly acting as an electron reservoir instead of a photosensitizer. This offers a novel understanding of the essential roles of GQDs when used in hybrid photocatalysts for photocatalytic applications (Figure 9).

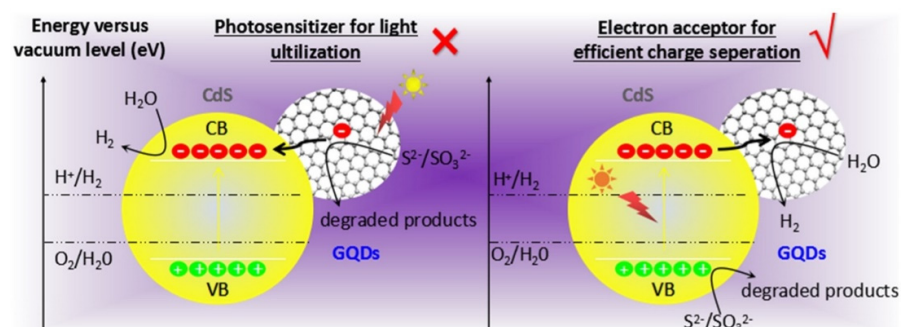


Figure 9. Photocatalytic mechanism of the $CdS/GQDs$ nanohybrids. Reprinted with permission from Ref. [111].

Gao et al. [62] studied the effects of QDs in QDs-modified hexagonal tubular carbon nitride. During photocatalysis, QDs play dual roles as a photosensitizer and an electron trap, which can extend the range of visible light absorption and inhibit the recombination of photoinduced charge carriers. Therefore, the composite exhibits a significantly higher photocatalytic efficiency, with a H₂ generation rate of 112.1 μmol/h; this value is about 9 times greater than that of pure carbon nitride. The abovementioned photocatalytic applications of CQDs all involve combinations with other semiconductors; in other words, CQDs work as cocatalysts in the photocatalytic H₂ generation reaction, while single CQDs have been reported to directly act as a photocatalyst. For instance, Yang et al. [112] reported that unmodified pure CQDs (3–4 nm) in the absence of a cocatalyst are also active in the photocatalytic hydrogen evolution reaction. The hydrogen evolution rate of CQDs can even reach 3615.3 μmol g⁻¹·h⁻¹, which is nearly 36 times that of the commercial P25 photocatalyst under identical conditions.

3. Summary and Outlook

In summary, quantum dots (QDs) have attracted considerable research attention from the scientific community. Compared to bulk materials, QDs exhibit various special properties, including band-gap tunability, an improved visible light absorption ability, and abundant surface active sites. Therefore, a great number of studies have reported on the application of QDs as efficient photocatalysts and cocatalysts for photocatalytic hydrogen production. This review provides a comprehensive description of the basic features of QDs, as well as their types and applications, in relation to photocatalytic hydrogen generation. Furthermore, semiconductor QDs serving as a single photocatalyst or in combination with other semiconductors for photocatalytic hydrogen production have been reviewed. Next, metal QDs and carbon QDs combined with other semiconductors for photocatalytic hydrogen production have also been discussed in detail. When optimized in terms of size distribution, shell materials and thickness, and surface ligands, QDs have excellent light absorption, exciton generation and charge separation properties. As such, QDs have been shown to be ideal components of photocatalysts. Although QDs-based hybrids exhibit an improved photocatalytic performance, the reported optimum photocatalytic efficiency is still not sufficient for large-scale industrial applications; thus, the new strategies set out to develop highly efficient QDs-based composites deserve more attention. Furthermore, the stability of QDs used in photocatalytic reaction processes is very important. QDs are often plagued by stability in use, which stems from the fact that there are always surface excitons. This leads to difficulties in reaching the ideal state during the cyclic testing of QDs. To overcome this drawback, the controlled assembly of two or more components has been investigated to enhance the stability of QDs' properties and structures, and to overcome some of the disadvantages of using single materials. As reported by Li et al. [113], CuO QDs were encapsulated in the pores of MIL-125(Ti) MOF and further combined with g-C₃N₄ to form a composite photocatalyst. Benefiting from the protection of the MIL-125(Ti) framework, the stability of the composite photocatalyst in the reaction system was significantly improved. In addition, the quantum confinement effects of QDs make them attractive for use in various applications, such as photocatalytic hydrogen generation, CO₂ photoreduction, optoelectronic applications, lithium-ion batteries, and solar cells. It can be observed that band energies can be tuned by controlling the particle sizes of QDs according to the quantum confinement effects of QDs, opening up new avenues to enhance the photocatalytic efficiency.

However, the design and study of QDs-based photocatalysts are still challenging as a result of several aspects, e.g., the up-conversion fluorescence effect of QDs, the structure–activity relationship and the structural engineering of QDs-based photocatalysts still need to be studied in depth. Future investigations may focus on the exploitation of novel QDs for efficient photocatalytic H₂ generation. In addition, the mechanisms determining the role of QDs in QDs-based hybrid photocatalysts are not very clear; in order to discern how they operate during photocatalytic reactions, more efforts must be made. Notably,

QDs-based hybrids are mainly investigated by use of a sacrificial donor; in short, the hydrogen evolution's half-reaction is under study. This is one of the more attractive and challenging topics that should be approached in future, in order to extend the application of QDs-based photocatalysts in efficient overall water splitting reactions to produce both hydrogen and oxygen.

Author Contributions: Conceptualization, X.G. and M.C.; validation, Q.W. and Y.L.; investigation, Q.W.; resources and writing—original draft preparation, X.G.; writing—review and editing, M.C.; visualization and funding acquisition, S.S. All authors have read and agreed to the published version of the manuscript.

Funding: This research was supported by the National Natural Science Foundation of China (22308001, 21902001, and 22179001), Higher Education Natural Science Foundation of Anhui Province (KJ2021A0029 and KJ2021A0027), Distinguished Young Research Project of Anhui Higher Education Institution (022AH020007), and The University Synergy Innovation Program of Anhui Province (GXXT-2023-009).

Data Availability Statement: The research data presented in this study are available upon request from the corresponding authors.

Conflicts of Interest: The authors have no conflicts of interest.

References

1. Ahmad, H.; Kamarudin, S.K.; Minggu, L.J.; Kassim, M. Hydrogen from photo-catalytic water splitting process: A review. *Renew. Sustain. Energy Rev.* **2015**, *43*, 599–610. [[CrossRef](#)]
2. Xie, G.C.; Zhang, K.; Guo, B.D.; Liu, Q.; Fang, L.; Gong, J.R. Graphene-Based Materials for Hydrogen Generation from Light-Driven Water Splitting. *Adv. Mater.* **2013**, *25*, 3820–3839. [[CrossRef](#)] [[PubMed](#)]
3. Liao, C.H.; Huang, C.W.; Wu, J.C.S. Hydrogen Production from Semiconductor-based Photocatalysis via Water Splitting. *Catalysts* **2012**, *2*, 490–516. [[CrossRef](#)]
4. Li, Y.; Zhang, J.Z. Hydrogen generation from photoelectrochemical water splitting based on nanomaterials. *Laser Photon. Rev.* **2010**, *4*, 517–528. [[CrossRef](#)]
5. Shangguan, W.F. Hydrogen evolution from water splitting on nanocomposite photocatalysts. *Sci. Technol. Adv. Mater.* **2017**, *8*, 76–81. [[CrossRef](#)]
6. Yuan, Y.P.; Ruan, L.W.; Barber, J.; Joachim Loo, S.C.; Xue, C. Hetero-nanostructured suspended photocatalysts for solar-to-fuel conversion. *Energy Environ. Sci.* **2014**, *7*, 3934–3951. [[CrossRef](#)]
7. Chen, S.; Takata, T.; Domen, K. Particulate photocatalysts for overall water splitting. *Nat. Rev. Mater.* **2017**, *2*, 17050. [[CrossRef](#)]
8. Chen, X.B.; Shen, S.H.; Guo, L.J.; Mao, S.S. Semiconductor-based Photocatalytic Hydrogen Generation. *Chem. Rev.* **2010**, *110*, 6503–6570. [[PubMed](#)]
9. Kudo, A.; Miseki, Y. Heterogeneous photocatalyst materials for water splitting. *Chem. Soc. Rev.* **2009**, *38*, 253–278. [[CrossRef](#)]
10. Ran, J.; Zhang, J.; Yu, J.; Jaroniec, M.; Qiao, S.Z. Earth-abundant cocatalysts for semiconductor-based photocatalytic water splitting. *Chem. Soc. Rev.* **2014**, *43*, 7787–7812. [[CrossRef](#)]
11. Hisatomi, T.; Kubota, J.; Domen, K. Recent advances in semiconductors for photocatalytic and photoelectrochemical water splitting. *Chem. Soc. Rev.* **2014**, *43*, 7520–7535. [[CrossRef](#)] [[PubMed](#)]
12. Fang, Z.; Wang, Y.; Song, J.; Sun, Y.; Zhou, J.; Xu, R.; Duan, H. Immobilizing CdS quantum dots and dendritic Pt nanocrystals on thiolated graphene nanosheets toward highly efficient photocatalytic H₂ evolution. *Nanoscale* **2013**, *5*, 9830–9838. [[CrossRef](#)]
13. Ge, L.; Zuo, F.; Liu, J.; Ma, Q.; Wang, C.; Sun, D.; Bartels, L.; Feng, P. Synthesis and Efficient Visible Light Photocatalytic Hydrogen Evolution of Polymeric g-C₃N₄ Coupled with CdS Quantum Dots. *J. Phys. Chem.* **2012**, *116*, 13708–13714. [[CrossRef](#)]
14. Rao, V.N.; Reddy, N.L.; Kumari, M.M.; Cheralathan, K.K.; Ravi, P.; Sathish, M.; Neppolian, B.; Reddy, K.R.; Shetti, N.P.; Prathap, P.; et al. Sustainable hydrogen production for the greener environment by quantum dots-based efficient photocatalysts: A review. *J. Environ. Manag.* **2019**, *248*, 109246. [[CrossRef](#)] [[PubMed](#)]
15. Li, X.-B.; Tung, C.-H.; Wu, L.-Z. Semiconducting quantum dots for artificial photosynthesis. *Nat. Rev. Chem.* **2018**, *2*, 160–173. [[CrossRef](#)]
16. Albero, J.; Clifford, J.N.; Palomares, E. Quantum dot based molecular solar cells. *Coord. Chem. Rev.* **2014**, *263–264*, 53–64. [[CrossRef](#)]
17. Fan, X.B.; Yu, S.; Hou, B.; Kim, J.M. Quantum Dots Based Photocatalytic Hydrogen Evolution. *Isr. J. Chem.* **2019**, *59*, 762–773. [[CrossRef](#)]
18. Kandi, D.; Martha, S.; Parida, K.M. Quantum dots as enhancer in photocatalytic hydrogen evolution: A review. *Int. J. Hydrogen Energy* **2017**, *42*, 9467–9481. [[CrossRef](#)]
19. Freeman, R.; Willner, I. Optical molecular sensing with semiconductor quantum dots (QDs). *Chem. Soc. Rev.* **2012**, *41*, 4067–4085. [[CrossRef](#)]

20. Li, X.B.; Tung, C.H.; Wu, L.Z. Quantum Dot Assembly for Light-Driven Multielectron Redox Reactions, such as Hydrogen Evolution and CO₂ Reduction. *Angew. Chem.-Int. Edit.* **2019**, *58*, 10804–10811. [[CrossRef](#)]
21. Pirsaeheb, M.; Asadi, A.; Sillanpää, M.; Farhadian, N. Application of carbon quantum dots to increase the activity of conventional photocatalysts: A systematic review. *J. Mol. Liq.* **2018**, *271*, 857–871. [[CrossRef](#)]
22. Sui, Y.; Wu, L.; Zhong, S.; Liu, Q. Carbon quantum dots/TiO₂ nanosheets with dominant (001) facets for enhanced photocatalytic hydrogen evolution. *Appl. Surf. Sci.* **2019**, *480*, 810–816. [[CrossRef](#)]
23. Chu, K.W.; Lee, S.L.; Chang, C.J.; Liu, L. Recent Progress of Carbon Dot Precursors and Photocatalysis Applications. *Polymers* **2019**, *11*, 689. [[CrossRef](#)] [[PubMed](#)]
24. Li, K.; Su, F.Y.; Zhang, W.-D. Modification of g-C₃N₄ nanosheets by carbon quantum dots for highly efficient photocatalytic generation of hydrogen. *Appl. Surf. Sci.* **2016**, *375*, 110–117. [[CrossRef](#)]
25. Yu, H.; Shi, R.; Zhao, Y.; Waterhouse, G.I.; Wu, L.Z.; Tung, C.H.; Zhang, T. Smart Utilization of Carbon Dots in Semiconductor Photocatalysis. *Adv. Mater.* **2016**, *28*, 9454–9477. [[CrossRef](#)]
26. Jin, X.; Fan, X.; Tian, J.; Cheng, R.; Li, M.; Zhang, L. MoS₂ quantum dot decorated g-C₃N₄ composite photocatalyst with enhanced hydrogen evolution performance. *RSC Adv.* **2016**, *6*, 52611–52619. [[CrossRef](#)]
27. Fernando, K.A.S.; Sahu, S.; Liu, Y.; Lewis, W.K.; Gulians, E.A.; Jafariyan, A.; Wang, P.; Bunker, C.E.; Sun, Y.-P. Carbon Quantum Dots and Applications in Photocatalytic Energy Conversion. *ACS Appl. Mater. Interfaces* **2015**, *7*, 8363–8376. [[CrossRef](#)]
28. Wang, Y.; Liu, X.; Liu, J.; Han, B.; Hu, X.; Yang, F.; Xu, Z.; Li, Y.; Jia, S.; Li, Z.; et al. Carbon Quantum Dot Implanted Graphite Carbon Nitride Nanotubes: Excellent Charge Separation and Enhanced Photocatalytic Hydrogen Evolution. *Angew. Chem. Int. Ed.* **2018**, *57*, 5765–5771. [[CrossRef](#)]
29. Sargin, I.; Yanalak, G.; Arslan, G.; Patir, I.H. Green synthesized carbon quantum dots as TiO₂ sensitizers for photocatalytic hydrogen evolution. *Int. J. Hydrogen Energy* **2019**, *44*, 21781–21789. [[CrossRef](#)]
30. Yu, H.; Zhao, Y.; Zhou, C.; Shang, L.; Peng, Y.; Cao, Y.; Wu, L.-Z.; Tung, C.-H.; Zhang, T. Carbon quantum dots/TiO₂ composites for efficient photocatalytic hydrogen evolution. *J. Mater. Chem. A* **2014**, *2*, 3344–3351. [[CrossRef](#)]
31. Jia, X.; Li, J.; Wang, E. One-pot green synthesis of optically pH-sensitive carbon dots with upconversion luminescence. *Nanoscale* **2012**, *4*, 5572–5575. [[CrossRef](#)] [[PubMed](#)]
32. Wang, Y.; Hu, A. Carbon quantum dots: Synthesis, properties and applications. *J. Mater. Chem. C* **2014**, *2*, 6921–6939. [[CrossRef](#)]
33. Chen, J.; Lv, S.; Shen, Z.; Tian, P.; Chen, J.; Li, Y. Novel ZnCdS Quantum Dots Engineering for Enhanced Visible-Light-Driven Hydrogen Evolution. *ACS Sustain. Chem. Eng.* **2019**, *7*, 13805–13814. [[CrossRef](#)]
34. Fan, X.-B.; Yu, S.; Zhan, F.; Li, Z.-J.; Gao, Y.J.; Li, X.B.; Zhang, L.P.; Tao, Y.; Tung, C.H. Nonstoichiometric Cu_xIn_yS Quantum Dots for Efficient Photocatalytic Hydrogen Evolution. *ChemSusChem* **2017**, *10*, 4833–4838. [[CrossRef](#)]
35. Han, J.S.; Liu, Y.; Wang, Y.; Zhao, R.Y.; Wang, L. Construction of ternary Cd_xMo_{1-x}Se quantum dots for enhanced photocatalytic hydrogen production. *J. Mater. Sci.* **2020**, *55*, 1117–1125. [[CrossRef](#)]
36. Jiang, Z.; Zhang, X.; Yang, G.; Yuan, Z.; Ji, X.; Kong, F.; Huang, B.; Dionysiou, D.D.; Chen, J. Hydrogel as a miniature hydrogen production reactor to enhance photocatalytic hydrogen evolution activities of CdS and ZnS quantum dots derived from modified gel crystal growth method. *Chem. Eng. J.* **2019**, *373*, 814–820. [[CrossRef](#)]
37. Liu, Y.; Dai, F.X.; Zhao, R.Y.; Huai, X.D.; Han, J.S.; Wang, L. Aqueous synthesis of core/shell/shell CdSe/CdS/ZnS quantum dots for photocatalytic hydrogen generation. *J. Mater. Sci.* **2019**, *54*, 8571–8580. [[CrossRef](#)]
38. Zhong, Y.; Chen, W.; Yu, S.; Xie, Z.; Wei, S.; Zhou, Y. CdSe Quantum Dots/g-C₃N₄ Heterostructure for Efficient H₂ Production under Visible Light Irradiation. *ACS Omega* **2018**, *3*, 17762–17769. [[CrossRef](#)] [[PubMed](#)]
39. Li, W.; Han, J.; Wu, Y.; Xiang, Q.; Qiao, Y.; Feng, C.; Chen, Z.; Deng, X. In-situ synthesis of CdS quantum dots on CdCO₃ cubic structure for enhanced photocatalytic hydrogen production performance. *Mater. Lett.* **2019**, *255*, 126560. [[CrossRef](#)]
40. Pan, Y.X.; Zhuang, H.; Hong, J.; Fang, Z.; Liu, H.; Liu, B.; Huang, Y.; Xu, R. Cadmium Sulfide Quantum Dots Supported on Gallium and Indium Oxide for Visible-Light-Driven Hydrogen Evolution from Water. *ChemSuschem* **2014**, *7*, 2537–2544. [[CrossRef](#)]
41. Zheng, Y.; Chen, Y.; Gao, B.; Chen, J.; Du, Z.; Lin, B. Polymeric carbon nitride hybridized by CuInS₂ quantum dots for photocatalytic hydrogen evolution. *Mater. Lett.* **2019**, *254*, 81–84. [[CrossRef](#)]
42. Liu, X.Y.; Chen, H.; Wang, R.L.; Shang, Y.Q.; Zhang, Q.; Li, W.; Zhang, G.Z.; Su, J.; Dinh, C.T.; Arquer, F.P.G.; et al. 0D-2D Quantum Dot: Metal Dichalcogenide Nanocomposite Photocatalyst Achieves Efficient Hydrogen Generation. *Adv. Mater.* **2017**, *29*, 1605646. [[CrossRef](#)] [[PubMed](#)]
43. Zhong, Y.; Shao, Y.; Ma, F.; Wu, Y.; Huang, B.; Hao, X. Band-gap-matched CdSe QD/WS₂ nanosheet composite: Size-controlled photocatalyst for high-efficiency water splitting. *Nano Energy* **2017**, *31*, 84–89. [[CrossRef](#)]
44. Wang, P.; Wang, M.; Zhang, J.; Li, C.; Xu, X.; Jin, Y. Shell Thickness Engineering Significantly Boosts the Photocatalytic H₂ Evolution Efficiency of CdS/CdSe Core/Shell Quantum Dots. *ACS Appl. Mater. Interfaces* **2017**, *9*, 35712–35720. [[CrossRef](#)] [[PubMed](#)]
45. Xue, F.; Liu, M.C.; Cheng, C.; Deng, J.K.; Shi, J.W. Localized NiS₂ Quantum Dots on g-C₃N₄ Nanosheets for Efficient Photocatalytic Hydrogen Production from Water. *Chemcatchem* **2018**, *10*, 5441–5448. [[CrossRef](#)]
46. Liu, Y.; Li, C.F.; Li, X.Y.; Yu, W.B.; Dong, W.-D.; Zhao, H.; Hu, Z.-Y.; Deng, Z.; Wang, C.; Wu, S.-J.; et al. Molybdenum disulfide quantum dots directing zinc indium sulfide heterostructures for enhanced visible light hydrogen production. *J. Colloid Interface Sci.* **2019**, *551*, 111–118. [[CrossRef](#)] [[PubMed](#)]

47. Zhang, N.; Shi, J.; Mao, S.S.; Guo, L. Co₃O₄ quantum dots: Reverse micelle synthesis and visible-light-driven photocatalytic overall water splitting. *Chem. Commun.* **2014**, *50*, 2002–2004. [[CrossRef](#)] [[PubMed](#)]
48. Yang, H.; Yin, J.; Cao, R.; Sun, P.; Zhang, S.; Xu, X. Constructing highly dispersed 0D Co₃S₄ quantum dots/2D g-C₃N₄ nanosheets nanocomposites for excellent photocatalytic performance. *Sci. Bull.* **2019**, *64*, 1510–1517. [[CrossRef](#)] [[PubMed](#)]
49. Liu, J.; Ke, J.; Li, Y.; Liu, B.; Wang, L.; Xiao, H.; Wang, S. Co₃O₄ quantum dots/TiO₂ nanobelt hybrids for highly efficient photocatalytic overall water splitting. *Appl. Catal. B-Environ.* **2018**, *236*, 396–403. [[CrossRef](#)]
50. Hong, W.; Zhou, Y.; Lv, C.; Han, Z.; Chen, G. NiO Quantum Dot Modified TiO₂ toward Robust Hydrogen Production Performance. *ACS Sustain. Chem. Eng.* **2018**, *6*, 889–896. [[CrossRef](#)]
51. Liang, Z.; Dong, X.; Han, Y.; Geng, J. In-situ growth of 0D/2D Ni₂P quantum dots/red phosphorus nanosheets with p-n heterojunction for efficient photocatalytic H₂ evolution under visible light. *Appl. Surf. Sci.* **2019**, *484*, 293–299. [[CrossRef](#)]
52. Lu, Z.; Li, C.; Han, J.; Wang, L.; Wang, S.; Ni, L.; Wang, Y. Construction 0D/2D heterojunction by highly dispersed Ni₂P QDs loaded on the ultrathin g-C₃N₄ surface towards super high photocatalytic and photoelectric performance. *Appl. Catal. B-Environ.* **2018**, *237*, 919–926. [[CrossRef](#)]
53. Li, Y.; Ding, L.; Guo, Y.; Liang, Z.; Cui, H.; Tian, J. Boosting the Photocatalytic Ability of g-C₃N₄ for Hydrogen Production by Ti₃C₂ MXene Quantum Dots. *ACS Appl. Mater. Interfaces* **2019**, *11*, 41440–41447. [[CrossRef](#)]
54. Kuang, P.Y.; Zheng, P.X.; Liu, Z.Q.; Lei, J.L.; Wu, H.; Li, N.; Ma, T.-Y. Embedding Au Quantum Dots in Rimous Cadmium Sulfide Nanospheres for Enhanced Photocatalytic Hydrogen Evolution. *Small* **2016**, *12*, 6735–6744. [[CrossRef](#)] [[PubMed](#)]
55. Chen, T.; Quan, W.; Yu, L.; Hong, Y.; Song, C.; Fan, M.; Xiao, L.; Gu, W.; Shi, W. One-step synthesis and visible-light-driven H₂ production from water splitting of Ag quantum dots/g-C₃N₄ photocatalysts. *J. Alloys Compd.* **2016**, *686*, 628–634. [[CrossRef](#)]
56. Wang, K.; Wang, X.; Pan, H.; Liu, Y.; Xu, S.; Cao, S. In situ fabrication of CDs/g-C₃N₄ hybrids with enhanced interface connection via calcination of the precursors for photocatalytic H₂ evolution. *Int. J. Hydrogen Energy* **2018**, *43*, 91–99. [[CrossRef](#)]
57. Gao, Y.; Hou, F.; Hu, S.; Wu, B.; Wang, Y.; Zhang, H.; Jiang, B.; Fu, H. Graphene Quantum-Dot-Modified Hexagonal Tubular Carbon Nitride for Visible-Light Photocatalytic Hydrogen Evolution. *ChemCatChem* **2018**, *10*, 1330–1335. [[CrossRef](#)]
58. Qin, J.; Zeng, H. Photocatalysts fabricated by depositing plasmonic Ag nanoparticles on carbon quantum dots/graphitic carbon nitride for broad spectrum photocatalytic hydrogen generation. *Appl. Catal. B-Environ.* **2017**, *209*, 161–173. [[CrossRef](#)]
59. Devarayapalli, K.C.; Zeng, J.; Lee, D.S.; Vattikuti, S.V.P.; Shim, J. In-situ Pt nanoparticles decorated BiOBr heterostructure for enhanced visible light-based photocatalytic activity: Synergistic effect. *Chemosphere* **2022**, *298*, 134125. [[CrossRef](#)]
60. Zhang, B.; Chen, C.; Liu, J.; Qiao, W.; Zhao, J.; Yang, J.; Yu, Y.; Chen, S.; Qin, Y. Simultaneous Ni nanoparticles decoration and Ni doping of CdS nanorods for synergistically promoting photocatalytic H₂ evolution. *Appl. Surf. Sci.* **2020**, *508*, 144869. [[CrossRef](#)]
61. Mao, S.; Zou, Y.; Sun, G.; Zeng, L.; Wang, Z.; Ma, D.; Guo, Y.; Cheng, Y.; Wang, C.; Shi, J.-W. Thio linkage between CdS quantum dots and UiO-66-type MOFs as an effective transfer bridge of charge carriers boosting visible-light-driven photocatalytic hydrogen production. *J. Colloid Interface Sci.* **2021**, *581*, 1–10. [[CrossRef](#)] [[PubMed](#)]
62. Fan, Y.; Hu, J.; Li, T.; Xu, S.; Chen, S.; Yin, H. Enhanced photocatalytic hydrogen evolution through MoS₂ quantum dots modification of bismuth-based perovskites. *Chem. Commun.* **2024**, *60*, 1004. [[CrossRef](#)] [[PubMed](#)]
63. Chen, H.; Mo, Z.; Wang, Z.; Yan, P.; Sun, P.; Wu, G.; Zhang, J.; Zhu, X.; Wang, L.; Xu, H. Implanting nitrogen-doped graphene quantum dots on porous ultrathin carbon nitride for efficient metal-free photocatalytic hydrogen evolution. *J. Environ. Chem. Eng.* **2023**, *11*, 109801. [[CrossRef](#)]
64. Zhu, S.C.; Xiao, F.X. Transition Metal Chalcogenides Quantum Dots: Emerging Building Blocks toward Solar-to-Hydrogen Conversion. *ACS Catal.* **2023**, *13*, 7269–7309. [[CrossRef](#)]
65. Yuan, Y.J.; Chen, D.; Yu, Z.T.; Zou, Z.G. Cadmium sulfide-based nanomaterials for photocatalytic hydrogen production. *J. Mater. Chem. A* **2018**, *6*, 11606–11630. [[CrossRef](#)]
66. Wang, M.; Zhang, H.; Zu, H.; Zhang, Z.; Han, J. Construction of TiO₂/CdS heterojunction photocatalysts with enhanced visible light activity. *Appl. Surf. Sci.* **2018**, *455*, 729–735. [[CrossRef](#)]
67. Chen, W.; Wang, Y.; Liu, M.; Gao, L.; Mao, L.; Fan, Z.; Shangguan, W. In situ photodeposition of cobalt on CdS nanorod for promoting photocatalytic hydrogen production under visible light irradiation. *Appl. Surf. Sci.* **2018**, *444*, 485–490. [[CrossRef](#)]
68. Wang, P.; Wu, T.; Ao, Y.; Wang, C. Fabrication of noble-metal-free CdS nanorods-carbon layer-cobalt phosphide multiple heterojunctions for efficient and robust photocatalyst hydrogen evolution under visible light irradiation. *Renew. Energy* **2019**, *131*, 180–186. [[CrossRef](#)]
69. Huang, L.; Yang, J.; Wang, X.; Han, J.; Han, H.; Li, C. Effects of surface modification on photocatalytic activity of CdS nanocrystals studied by photoluminescence spectroscopy. *Phys. Chem. Chem. Phys.* **2013**, *15*, 553–560. [[CrossRef](#)]
70. Yu, H.; Huang, Y.; Gao, D.; Wang, P.; Tang, H. Improved H₂-generation performance of Pt/CdS photocatalyst by a dual-function TiO₂ mediator for effective electron transfer and hole blocking. *Ceram. Int.* **2019**, *45*, 9807–9813. [[CrossRef](#)]
71. Zheng, D.; Zhang, G.; Wang, X. Integrating CdS quantum dots on hollow graphitic carbon nitride nanospheres for hydrogen evolution photocatalysis. *Appl. Catal. B-Environ.* **2015**, *179*, 479–488. [[CrossRef](#)]
72. Hou, J.; Yang, C.; Cheng, H.; Wang, Z.; Jiao, S.; Zhu, H. Ternary 3D architectures of CdS QDs/graphene/ZnIn₂S₄ heterostructures for efficient photocatalytic H₂ production. *Phys. Chem. Chem. Phys.* **2013**, *15*, 15660–15668. [[CrossRef](#)] [[PubMed](#)]
73. Fan, X.-B.; Yu, S.; Wang, X.; Li, Z.-J.; Zhan, F.; Li, J.-X.; Gao, Y.-J.; Xia, A.-D.; Tao, Y.; Li, X.-B.; et al. Susceptible Surface Sulfide Regulates Catalytic Activity of CdSe Quantum Dots for Hydrogen Photogeneration. *Adv. Mater.* **2019**, *31*, 1804872. [[CrossRef](#)] [[PubMed](#)]

74. Li, C.R.; Lei, Y.L.; Li, H.; Ni, M.; Yang, D.R.; Xie, X.Y.; Wang, Y.F.; Ma, H.B.; Xu, W.G.; Xia, X.H. Suppressing Non-Radiative Relaxation through Single-Atom Metal Modification for Enhanced Fluorescence Efficiency in Molybdenum Disulfide Quantum Dots. *Angew. Chem. Int. Ed.* **2022**, *61*, 1–7.
75. Yuan, Y.J.; Chen, D.Q.; Xiong, M.; Zhong, J.S.; Wan, Z.Y.; Zhou, Y.; Liu, S.; Yu, Z.T.; Yang, L.X.; Zou, Z.G. Bandgap engineering of $(\text{AgIn})_x\text{Zn}_{2(1-x)}\text{S}_2$ quantum dot photosensitizers for photocatalytic H_2 generation. *Appl. Catal. B-Environ.* **2017**, *204*, 58–66. [[CrossRef](#)]
76. Ma, Q.; Yue, H.X.; Zhu, Y.N.; Wang, J.P.; Che, Q.D.; Shi, R.X.; Yang, P. Synthesis and Optical Properties of $\text{CdTe}_x\text{Se}_{1-x}$ -Based Red to Near-Infrared Emitting Quantum Dots. *J. Nanosci. Nanotechnol.* **2015**, *15*, 4442–4449. [[CrossRef](#)] [[PubMed](#)]
77. Yang, F.H.; Yang, P.; Zhang, L.P. Synthesis of near-infrared-emitting CdTeSe and CdZnTeSe quantum dots. *Luminescence* **2013**, *28*, 836–841. [[CrossRef](#)] [[PubMed](#)]
78. Nguyen, A.T.; Lin, W.H.; Lu, Y.H.; Chiou, Y.D.; Hsu, Y.J. First demonstration of rainbow photocatalysts using ternary $\text{Cd}_{1-x}\text{Zn}_x\text{Se}$ nanorods of varying compositions. *Appl. Catal. A-Gen.* **2014**, *476*, 140–147. [[CrossRef](#)]
79. Xiao, M.; Hao, M.; Lyu, M.; Moore, E.G.; Zhang, C.; Luo, B.; Hou, J.; Lipton-Duffin, J.; Wang, L. Surface ligands stabilized lead halide perovskite quantum dot photocatalyst for visible light-driven hydrogen generation. *Adv. Funct. Mater.* **2019**, *29*, 1905683. [[CrossRef](#)]
80. Song, W.; Wang, Y.; Wang, C.; Wang, B.; Feng, J.; Luo, W.; Wu, C.; Yao, Y.; Zou, Z. Photocatalytic Hydrogen Production by Stable CsPbBr_3 @PANI Nanoparticles in Aqueous Solution. *ChemCatChem* **2021**, *13*, 1711. [[CrossRef](#)]
81. Li, T.L.; Cai, C.D.; Yeh, T.F.; Teng, H. Capped CuInS_2 quantum dots for H_2 evolution from water under visible light illumination. *J. Alloys Compd.* **2013**, *550*, 326–330. [[CrossRef](#)]
82. Zhu, H.; Song, N.; Lian, T. Controlling Charge Separation and Recombination Rates in CdSe/ZnS Type I Core-Shell Quantum Dots by Shell Thicknesses. *J. Am. Chem. Soc.* **2010**, *132*, 15038–15045. [[CrossRef](#)] [[PubMed](#)]
83. Li, Z.J.; Li, X.B.; Wang, J.J.; Yu, S.; Li, C.B.; Tung, C.H.; Wu, L.Z. A robust “artificial catalyst” in situ formed from CdTe QDs and inorganic cobalt salts for photocatalytic hydrogen evolution. *Energy Environ. Sci.* **2013**, *6*, 465–469. [[CrossRef](#)]
84. Li, J.J.; Wang, Y.A.; Guo, W.Z.; Keay, J.C.; Mishima, T.D.; Johnson, M.B.; Peng, X.G. Large-scale synthesis of nearly monodisperse CdSe/CdS core/shell nanocrystals using air-stable reagents via successive ion layer adsorption and reaction. *J. Am. Chem. Soc.* **2003**, *125*, 12567–12575. [[CrossRef](#)] [[PubMed](#)]
85. Cao, S.W.; Yuan, Y.P.; Fang, J.; Shahjamali, M.M.; Boey, F.Y.C.; Barber, J.; Loo, S.C.J.; Xue, C. In-situ growth of CdS quantum dots on $g\text{-C}_3\text{N}_4$ nanosheets for highly efficient photocatalytic hydrogen generation under visible light irradiation. *Int. J. Hydrogen Energy* **2013**, *38*, 1258–1266.
86. Jiao, Y.; Huang, Q.; Wang, J.; He, Z.; Li, Z. A Novel MoS_2 Quantum Dots (QDs) Decorated Z-Scheme $g\text{-C}_3\text{N}_4$ Nanosheet/N-Doped Carbon Dots Heterostructure Photocatalyst for Photocatalytic Hydrogen Evolution. *Appl. Catal. B Environ. Energy* **2019**, *247*, 124–132. [[CrossRef](#)]
87. Zhu, Y.; Wang, Y.; Chen, Z.; Qin, L.; Yang, L.; Zhu, L.; Tang, P.; Gao, T.; Huang, Y.; Sha, Z.; et al. Visible light induced photocatalysis on CdS quantum dots decorated TiO_2 nanotube arrays. *Appl. Catal. A-Gen.* **2015**, *498*, 159–166. [[CrossRef](#)]
88. Chen, W.; Yu, S.; Zhong, Y.; Fan, X.-B.; Wu, L.-Z.; Zhou, Y. Effect of electron transfer on the photocatalytic hydrogen evolution efficiency of faceted TiO_2/CdSe QDs under visible light. *New J. Chem.* **2018**, *42*, 4811–4817. [[CrossRef](#)]
89. Yu, J.; Zhang, J.; Jaroniec, M. Preparation and enhanced visible-light photocatalytic H_2 -production activity of CdS quantum dots-sensitized $\text{Zn}_{1-x}\text{Cd}_x\text{S}$ solid solution. *Green Chem.* **2010**, *12*, 1611–1614. [[CrossRef](#)]
90. Thibert, A.; Frame, F.A.; Busby, E.; Holmes, M.A.; Osterloh, F.E.; Larsen, D.S. Sequestering High-Energy Electrons to Facilitate Photocatalytic Hydrogen Generation in CdSe/CdS Nanocrystals. *J. Phys. Chem. Lett.* **2011**, *2*, 2688–2694. [[CrossRef](#)]
91. Reddy, N.L.; Emin, S.; Valant, M.; Shankar, M.V. Nanostructured Bi_2O_3 @ TiO_2 photocatalyst for enhanced hydrogen production. *Int. J. Hydrogen Energy* **2017**, *42*, 6627–6636. [[CrossRef](#)]
92. Pan, L.; Zhang, J.W.; Jia, X.; Ma, Y.H.; Zhang, X.W.; Wang, L.; Zou, J.J. Highly efficient Z-scheme WO_{3-x} quantum dots/ TiO_2 for photocatalytic hydrogen generation. *Chin. J. Catal.* **2017**, *38*, 253–259. [[CrossRef](#)]
93. Su, H.; Wang, W.; Shi, R.; Tang, H.; Sun, L.; Wang, L.; Liu, Q.; Zhang, T. Recent Advances in Quantum Dot Catalysts for Hydrogen Evolution: Synthesis, Characterization, and Photocatalytic Application. *Carbon Energy* **2023**, *5*, e280. [[CrossRef](#)]
94. Nann, T.; Ibrahim, S.K.; Woi, P.-M.; Xu, S.; Ziegler, J.; Pickett, C.J. Water Splitting by Visible Light: A Nanophotocathode for Hydrogen Production. *Angew. Chem.-Int. Edit.* **2010**, *49*, 1574–1577. [[CrossRef](#)] [[PubMed](#)]
95. Jia, G.; Sun, M.; Wang, Y.; Cui, X.; Huang, B.; Yu, J.C. Enabling Efficient Photocatalytic Hydrogen Evolution via In Situ Loading of Ni Single Atomic Sites on Red Phosphorus Quantum Dots. *Adv. Funct. Mater.* **2022**, *33*, 2212051. [[CrossRef](#)]
96. Yu, S.; Fan, X.B.; Wang, X.; Li, J.G.; Zhang, Q.; Xia, A.; Wei, S.Q.; Wu, L.Z.; Zhou, Y.; Patzke, G.R. Efficient photocatalytic hydrogen evolution with ligand engineered all-inorganic InP and InP/ZnS colloidal quantum dots. *Nat. Commun.* **2018**, *9*, 4009. [[CrossRef](#)]
97. Yu, S.; Xie, Z.H.; Ran, M.X.; Wu, F.; Zhong, Y.Q.; Dan, M.; Zhou, Y.; Patzke, G.R. Zinc ions modified InP quantum dots for enhanced photocatalytic hydrogen evolution from hydrogen sulfide. *J. Colloid. Interf. Sci.* **2020**, *573*, 71–77. [[CrossRef](#)] [[PubMed](#)]
98. Pang, J.; Mendes, R.G.; Bachmatiuk, A.; Zhao, L.; Ta, H.Q.; Gemming, T.; Liu, H.; Liu, Z.; Rummeli, M.H. Applications of 2D MXenes in energy conversion and storage systems. *Chem. Soc. Rev.* **2019**, *48*, 72–133. [[CrossRef](#)]
99. Li, Z.; Wu, Y. 2D Early Transition Metal Carbides (MXenes) for Catalysis. *Small* **2019**, *15*, e1804736. [[CrossRef](#)]
100. Gao, G.; Mullane, A.P.O.; Du, A. 2D MXenes: A New Family of Promising Catalysts for the Hydrogen Evolution Reaction. *ACS Catal.* **2016**, *7*, 494–500. [[CrossRef](#)]

101. Zhou, C.; Tan, K.B.; Han, W.; Wang, L.; Lu, M. A Review of MXene-Derived Quantum Dots: Synthesis, Characterization, Properties, and Applications. *Particuology* **2024**, *91*, 50–57. [[CrossRef](#)]
102. Liang, X.; Liang, B.L.; Pan, Z.H.; Lang, X.F.; Zhang, Y.G.; Wang, G.S.; Yin, P.G.; Guo, L. Tuning plasmonic and chemical enhancement for SERS detection on graphene-based Au hybrids. *Nanoscale* **2015**, *7*, 20188–20196. [[CrossRef](#)] [[PubMed](#)]
103. Liu, Z.W.; Hou, W.B.; Pavaskar, P.; Aykol, M.; Cronin, S.B. Plasmon Resonant Enhancement of Photocatalytic Water Splitting Under Visible Illumination. *Nano Lett.* **2011**, *11*, 1111–1116. [[CrossRef](#)] [[PubMed](#)]
104. Ma, X.; Zhao, K.; Tang, H.J.; Chen, Y.; Lu, C.G.; Liu, W.; Gao, Y.; Zhao, H.J.; Tang, Z.Y. New Insight into the Role of Gold Nanoparticles in Au@CdS Core-Shell Nanostructures for Hydrogen Evolution. *Small* **2014**, *10*, 4664–4670. [[CrossRef](#)] [[PubMed](#)]
105. Zhang, G.; Lan, Z.A.; Lin, L.; Lin, S.; Wang, X. Overall water splitting by Pt/g-C₃N₄ photocatalysts without using sacrificial agents. *Chem. Sci.* **2016**, *7*, 3062–3066. [[CrossRef](#)] [[PubMed](#)]
106. Zhukovskyi, M.; Tongying, P.; Yashan, H.; Wang, Y.; Kuno, M. Efficient Photocatalytic Hydrogen Generation from Ni Nanoparticle Decorated CdS Nanosheets. *ACS Catal.* **2015**, *5*, 6615–6623. [[CrossRef](#)]
107. Babu, B.; Cho, M.; Byon, C.; Shim, J. One pot synthesis of Ag-SnO₂ quantum dots for highly enhanced sunlight-driven photocatalytic activity. *J. Alloys Compd.* **2018**, *731*, 162–171. [[CrossRef](#)]
108. Yu, S.; Zhong, Y.Q.; Yu, B.Q.; Cai, S.Y.; Wu, L.Z.; Zhou, Y. Graphene quantum dots to enhance the photocatalytic hydrogen evolution efficiency of anatase TiO₂ with exposed {001} facet. *Phys. Chem. Chem. Phys.* **2016**, *18*, 20338–20344. [[CrossRef](#)] [[PubMed](#)]
109. Lv, S.; Deng, Y.; Liu, Q.; Fu, Z.; Liu, X.; Wang, M.; Xiao, Z.; Li, B.; Wang, L. Carbon-Quantum-Dots-Involved Fe/Co/Ni Phosphide Open Nanotubes for High Effective Seawater Electrochemical Decomposition. *Appl. Catal. B Environ. Energy* **2023**, *326*, 122403. [[CrossRef](#)]
110. Chen, Y.; Yu, S.; Zhong, Y.; Wang, Y.; Ye, J.; Zhou, Y. Study of Indium Phosphide Quantum Dots/Carbon Quantum Dots System for Enhanced Photocatalytic Hydrogen Production from Hydrogen Sulfide. *Processes* **2023**, *11*, 3160. [[CrossRef](#)]
111. Lei, Y.; Yang, C.; Hou, J.; Wang, F.; Min, S.; Ma, X.; Jin, Z.; Xu, J.; Lu, G.; Huang, K.-W. Strongly coupled CdS/graphene quantum dots nanohybrids for highly efficient photocatalytic hydrogen evolution: Unraveling the essential roles of graphene quantum dots. *Appl. Catal. B-Environ.* **2017**, *216*, 59–69. [[CrossRef](#)]
112. Yang, P.; Zhao, J.; Wang, J.; Cui, H.; Li, L.; Zhu, Z. Pure carbon nanodots for excellent photocatalytic hydrogen generation. *RSC Adv.* **2015**, *5*, 21332–21335. [[CrossRef](#)]
113. Li, N.; Liu, X.; Zhou, J.; Chen, W.; Liu, M. Encapsulating CuO quantum dots in MIL-125(Ti) coupled with g-C₃N₄ for efficient photocatalytic CO₂ reduction. *Chem. Eng. J.* **2020**, *399*, 125782. [[CrossRef](#)]

Disclaimer/Publisher's Note: The statements, opinions and data contained in all publications are solely those of the individual author(s) and contributor(s) and not of MDPI and/or the editor(s). MDPI and/or the editor(s) disclaim responsibility for any injury to people or property resulting from any ideas, methods, instructions or products referred to in the content.